Available online at www.sciencedirect.com
ScienceDirect
Solid State Communications 145 (2008) 98–102
solid state communications
www.elsevier.com/locate/ssc

Size dependence of electronic and magnetic properties of double-perovskite Sr_2FeMoO_6

X.H. Li[a], Y.P. Sun[a,*], W.J. Lu[a], R. Ang[a], S.B. Zhang[a], X.B. Zhu[a], W.H. Song[a], J.M. Dai[a,b]

[a] *Key Laboratory of Materials Physics, Institute of Solid State Physics, Chinese Academy of Sciences, Hefei 230031, People's Republic of China*
[b] *Department of Physics, Huaibei Coal Industry Teachers' College, Huaibei 235000, People's Republic of China*

Received 4 July 2007; received in revised form 11 September 2007; accepted 15 October 2007 by B.-F. Zhu
Available online 23 October 2007

Abstract

Sr_2FeMoO_6 samples with different grain sizes were prepared by the sol–gel method. X-ray diffraction (XRD) patterns and field-emission scanning electron microscopy (FE-SEM) of the Sr_2FeMoO_6 samples show that the samples are in the nanometer range. The average grain sizes D for these samples are 34.5, 39.7 and 44.3 nm, increasing with the sintering temperature. The transport measurements show that the Sr_2FeMoO_6 samples behave like semiconductors at low temperatures, dominated by the carrier scattering at the grain boundaries (GBs). And the resistivities of the samples are 1.6, 1.2 and 0.5 mΩ cm at 10 K, respectively, increasing with decreasing grain size. The temperature dependences of the magnetization and resistance clearly demonstrate the coexistence of ferromagnetic metal and antiferromagnetic (or paramagnetic) insulator, which is believed to induce a metal–insulator transition at the Curie temperature (T_C).

PACS: 72.80.Ng; 75.30.Cr; 73.40.-c

Keywords: A. Sr_2FeMoO_6; B. Sol–gel method; D. Magnetoresistance

1. Introduction

Ideal half-metallic compounds having 100% spin-polarized carriers at the Fermi level have received much attention because of their potential applications in spintronics [1]. In 1998, Kobayashi et al. reported that Sr_2FeMoO_6 (SFMO), an oxide material of $A_2B'B''O_6$ type double-perovskite structure, where A is an alkaline-earth or rare-earth ion and the transition metal sites (perovskite B-sites) are occupied alternately by different cations B' and B'', is high in Curie temperature (T_C) and spin polarization [2]. And then, because of the room temperature ferromagnetism and low field magnetoresistance (MR) of SFMO, extensive work has been focused on the synthesis of the bulk materials [2–8] and thin films [9–12] as well as on research concerning the intrinsic physical properties. With the 100% spin-polarized property and the high Curie temperature, $T_C \sim 420$ K, of SFMO, the interaction between localized Fe 3d conduction electrons and delocalized electrons formed from Mo 4d–O 2p hybridized states has been proposed to explain the high conductivity, T_C, and spin polarization [2,3]. Based on these properties, there are a wide range of applications of the double-perovskite material SFMO.

For application in magnetic recording devices, a large MR at much lower fields over a wide temperature range is very desirable. But the large room temperature MR of SFMO can be achieved only in magnetic fields of a few teslas. So, we focus on reducing the field scale and increasing the operating temperature and the value of the MR for SFMO. The MR effect can be enhanced by decreasing the grain size and increasing the Fe/Mo ordering parameter S [6,13]. In this paper, to enhance the MR at room temperature and research into the grain boundary (GB) effect and the transport properties of T_C for SFMO polycrystalline materials, we have prepared SFMO bulk samples via the sol–gel method with different grain sizes on a nanometer scale. We find that the MR value increases with reduction of the grain size and the presence of a metal–insulator transition around T_C, which may be

* Corresponding author. Fax: +86 551 5591434.
E-mail address: ypsun@issp.ac.cn (Y.P. Sun).

0038-1098/$ - see front matter © 2007 Elsevier Ltd. All rights reserved.
doi:10.1016/j.ssc.2007.10.021

attributed to the coexistence of ferromagnetic metallic and antiferromagnetic (or paramagnetic) insulating domains.

2. Experiment

SFMO samples were prepared by the sol–gel method; and this preparation was followed by heat treatments at different temperatures. Strontium acetate [$Sr(CH_3COO)_2{\cdot}0.5H_2O$], ferric citrate [$Fe(C_6H_5O_7)$], ammonium molybdate [$(NH_4)_6Mo_7O_{24}{\cdot}4H_2O$] were mixed stoichiometrically with citric acid until a gel formed. The gel was dried at 80 °C, and then preheated at 500 °C for 6 h and 700 °C for 6 h. Finally, the powders were pulverized and made into pellets; and this was followed by sintering at different temperatures (800, 900 and 1000 °C) in a stream of 5% H_2 in a N_2 atmosphere for 5 h.

For ease of description, we define here the samples sintered at different temperatures (800, 900 and 1000 °C) as sample A, sample B, and sample C, respectively.

The crystal structure and the phase purity of all the samples were examined by means of powder x-ray diffraction (XRD), using a Philips X'pert PRO x-ray diffract meter Cu Kα radiation at room temperature. The microstructures were identified using an FEI designed Field-Emission Scanning Electron Microscope (FE-SEM). The magnetic measurements were carried out with a commercial Superconducting Quantum Interference Device (SQUID) system (Quantum Design MPMS) ($1.8\ \mathrm{K} \leq T \leq 400\ \mathrm{K}$, $0\ \mathrm{T} \leq H \leq 5\ \mathrm{T}$).

3. Results and discussion

Fig. 1 shows the XRD of the SFMO samples and the normalized XRD profiles of the (200) peak for the samples. The powder XRD at room temperature shows that sample B and sample C are single phase and sample A has some secondary phase $SrMoO_4$, which is similar to our previous results for SFMO, Ca_2FeMoO_6 bulk materials and films, which may be attributed to the relatively low H_2% and the low temperature in the annealing process [6,10,14]. The XRD patterns of the samples can be indexed with a tetragonal lattice with space group $I4/mmm$. The structural parameters and the occupancy of Fe at its correct site (g_{Fe}) are refined by the standard Rietveld technique and the fitting between the experimental spectra and calculated values is relatively good, based on the consideration of lower R_p (<1), R_{wp} and χ^2 values. And the values of the Fe/Mo ordering parameter S for the samples are 0.32, 0.44 and 0.51, respectively, which were calculated as $S = 2(g_{Fe} - 0.5)$ from g_{Fe} [7] and are shown in Table 1. The low value of S may be attributed to the use of the sol–gel method, the low sintering temperature and the short time of the sintering circuit. As an example, we have shown the experimental and calculated XRD patterns for sample B in Fig. 2. The unit-cell parameters of all the samples are shown in Table 1.

The average grain size D is estimated by means of the Scherrer formulation $D_{hkl} = k\lambda/B\cos\theta$, where D_{hkl} is the diameter of the particle, k is a constant (shape factor ~0.9) [6], B is the difference in width at half-height of the peaks between the measured sample and the standard of KCl used to calibrate

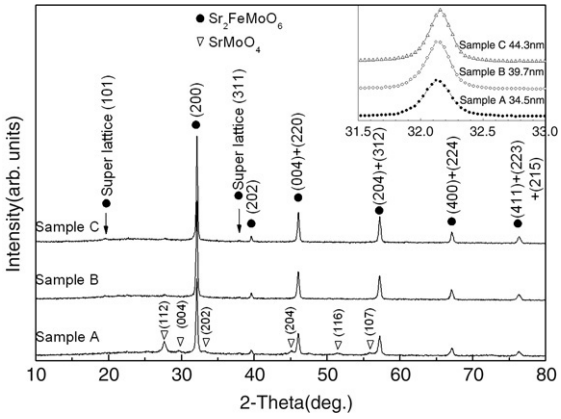

Fig. 1. The standard x-ray diffraction (XRD) θ–2θ patterns and the (200) diffraction peaks of Sr_2FeMoO_6 samples sintered at different temperatures.

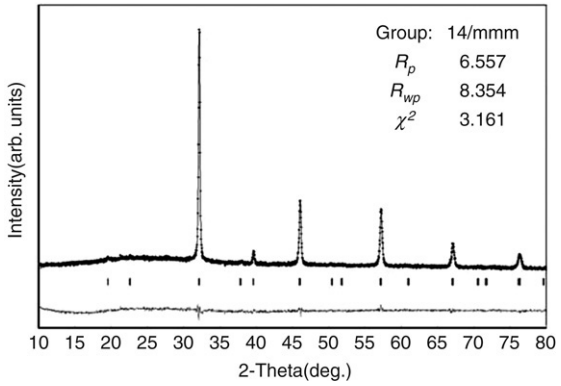

Fig. 2. XRD patterns of sample B. Crosses indicate the experimental data and the continuous line overlapping them the calculated data. The lowest curve shows the difference between experimental and calculated patterns. The vertical bars indicate the expected reflection positions.

Table 1
The lattice parameters, Curie temperature and saturation magnetization of the samples

Sample	A	B	C
R_p (%)	7.935	6.557	7.074
R_{wp} (%)	11.598	8.354	8.922
χ^2 (%)	6.954	3.161	3.502
a, b (Å)	5.5754	5.5747	5.5742
c (Å)	7.9003	7.9020	7.9042
$M_{S-300\ \mathrm{K}}$ (μ_B)	0.47	0.89	0.98
$M_{S-10\ \mathrm{K}}$ (μ_B)	1.25	1.62	1.93
T_C (K)	381	390	402
D (nm)	34.5	39.7	44.3
S	0.32	0.44	0.51

the intrinsic width associated with the equipment, and λ is the wavelength of the x-rays. The average grain sizes D for sample A, sample B and sample C are 34.5, 39.7 and 44.3 nm, respectively. The inset of Fig. 1 shows that the width at half-height of the peak decreases with the grain size increase.

The FE-SEM results for the SFMO samples are shown in Fig. 3. It can be seen that round grains with a diameter of about 50 nm are observed and all samples are homogeneous. As the

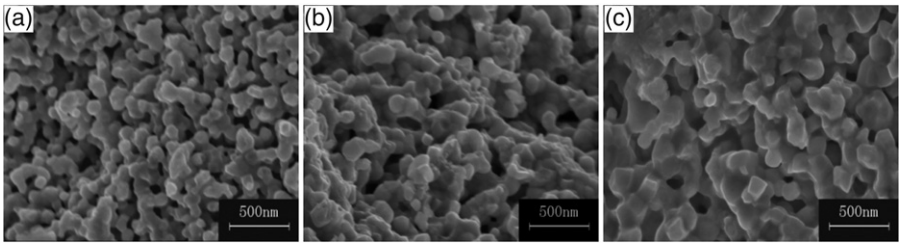

Fig. 3. The SEM images for Sr_2FeMoO_6 samples: (a) 800 °C, (b) 900 °C, (c) 1000 °C.

sintering temperature increases, the grain size becomes larger and the crystallization becomes more perfect.

The temperature dependence of the magnetization for the SFMO samples at 0.1 T is shown in Fig. 4. All the samples show a paramagnetic to ferromagnetic transition with temperature decrease. The T_C values for sample A, B and C are 381, 390, and 402 K, respectively, which is according to the valley of the first derivative of $M(T)$, $dM(T)/dT$. The values of T_C for the samples increase with the sintering temperature and are lower than those reported in the references [4,15], which may be attributed to the large density of the Fe/Mo disorder defects, as the value of T_C increases with the density of the Fe/Mo disorder defects decreasing [2,5,10,12]. For further study of the magnetic interaction, we fitted the experimental data in the paramagnetic region according to the Curie–Weiss law, $\chi = C/(T-\theta_P)$, where C is the Curie constant and θ_P is the Weiss temperature, as shown in the inset of Fig. 4. The fitted values of θ_P for the samples are 385, 392 and 398 K, respectively. The positive θ_P indicates the presence of a local ferromagnetic interaction. For these samples, it is found that the Curie–Weiss law is not in satisfactory agreement with the experimental curve from the temperature, T^*, which is higher than T_C. The deviation of the inverse susceptibility, $1/\chi$, from the high temperature straight line corresponding to noninteracting magnetic moments (Curie–Weiss behavior) marks the onset of the magnetic interaction between magnetic moments [16]. When the temperature is below T^*, the paramagnetic state becomes dominated by local ferromagnetic fluctuations that are presumably mediated by Fe^{3+}/Mo^{5+} hopping-induced double-exchange interactions.

The magnetization versus field $M(H)$ curves at 10 and 300 K for sample A, sample B and sample C are shown in Fig. 5. The values of the saturation magnetization of the samples at 300 K ($M_{S-300\,K}$) and 10 K ($M_{S-10\,K}$), as shown in Table 1, are less than 1.83 μ_B/f.u. at 300 K and 3.2 μ_B/f.u. at 10 K under an applied field of 0.5 T for a single crystal of SFMO [4]. This may be attributed to the high antisite defects. From the experimental data, $M_{S-10\,K}$, and the formula $M_S = 4*S$ at low temperature, we can obtain the values of the Fe/Mo ordering parameter S for the samples. They are 0.31, 0.41 and 0.48, respectively, similar to the values shown in Table 1. The density of the Fe/Mo disorder defects decreases with sintering temperature increase and the value of M_S increases with the density of the Fe/Mo disorder defects decreasing [9, 17]. So the values of M_S for the samples increase with sintering temperature increase.

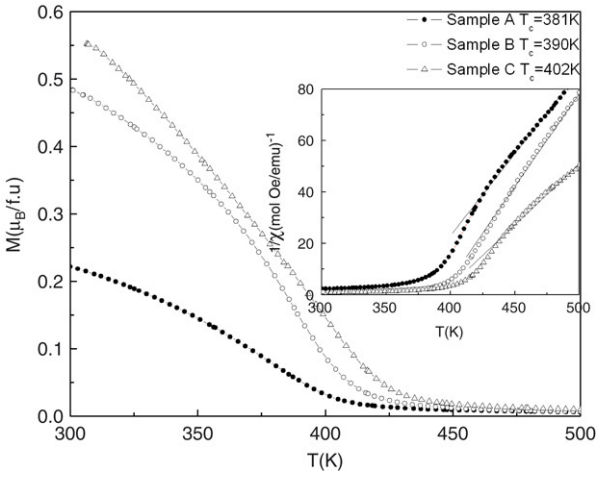

Fig. 4. The temperature dependence of the magnetization of the Sr_2FeMoO_6 samples at 0.1 T. The inset shows the inverse susceptibility as a function of temperature for the samples and the solid lines represent the fitting data according to the Curie–Weiss law.

Fig. 6 shows the temperature dependence of the resistivity for polycrystalline Sr_2FeMoO_6 at zero field in the temperature range from 10 to 450 K. At low temperatures, the resistivity decreases with temperature, and shows semiconductor behavior. A single crystal of SFMO should exhibit an intrinsic metallic state within the measured temperature range 5–350 K for high T_C above 400 K [4]. The influence of the grain boundaries cannot be eliminated by sintering at low temperature for a short time. So, the existence of grain boundaries causes the transport properties to depend on thermal scattering carriers, as commonly seen for polycrystalline ceramic samples [2]. The resistivities of the samples are 1.6, 1.2 and 0.5 mΩ cm at 10 K, respectively, increasing with decreasing grain size. And the values are larger than that for a single crystal of SFMO [4]. As we all know, grain size and the connections between the grains are very important for transport properties. Small grains and weak connection lead to a large amount of boundaries and interfaces; the higher resistivity for the sample with the smaller grain size is ascribed to the increase of the grain boundary contribution, which leads to more tunneling barriers for carrier transport [6,17]. For these samples, metal–insulator transition behavior is observed. The metal–insulator transition temperatures, T_P, of all the samples approach T_C. For the low temperature ($T < T_P$) ferromagnetic phase, a metallic behavior (ρ increases with temperature increase) is observed, while a semiconductor behavior (ρ decreases with temperature increase) is observed for the paramagnetic phase ($T > T_P$). We think that

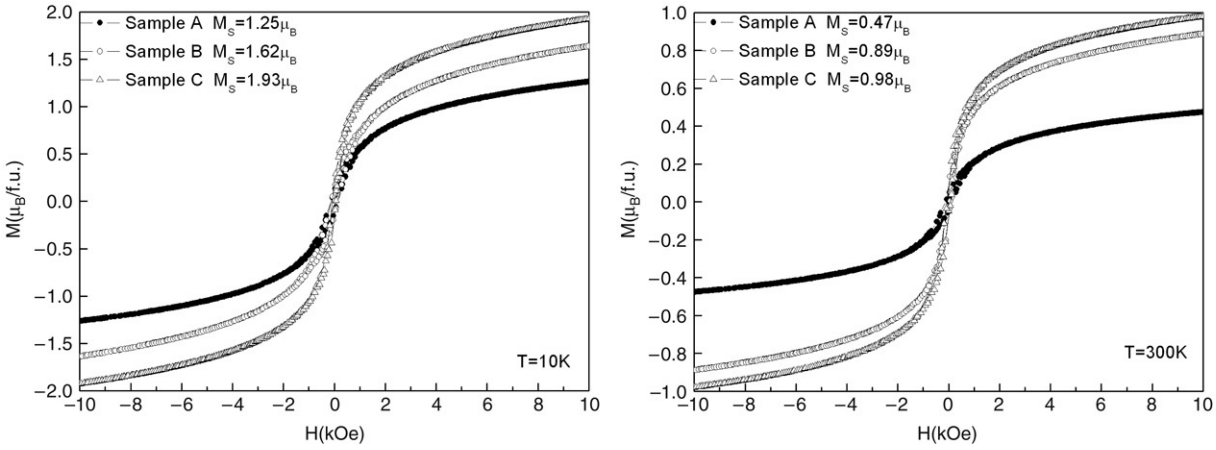

Fig. 5. The magnetic field dependence of the magnetization from −1 to +1 T.

this could be well understood from the phase separation scenario involving percolative transport through the ferromagnetic clusters in a background paramagnetic matrix. The ferromagnetic clusters are formed at T^* when the temperature decreases; the metallic state can be achieved and the size of clusters grows gradually until eventually transport through the ferromagnetic domains becomes possible [18]. The metallic behavior vanishes with increasing temperature, which originates from the ferromagnetic arrangement of spins, due to the spin arrangement deteriorating when the temperature increases [18].

We show the magnetic field dependences of the magnetoresistivity (MR) ratio, MR $= ([\rho(H) - \rho(0)]/\rho(0)) * 100\%$, from −5 to 5 T at 10 and 300 K in Fig. 7(a) and Fig. 7(b), respectively. It is seen that the MR value increases with reduction in grain size. And the values of the MR for the samples increase steeply in a low field region and increase more slowly with further increase in the field at low temperature, as shown in Fig. 7(a). But the value of MR at room temperature increases almost linearly with the field, as shown in Fig. 7(b). It is considered that the influence of the GB scattering is weaker on the field at high temperature, which leads to a small value and a linear dependence on the field of MR. The MR property of SFMO strongly depends on the density of the Fe/Mo disorder defects,

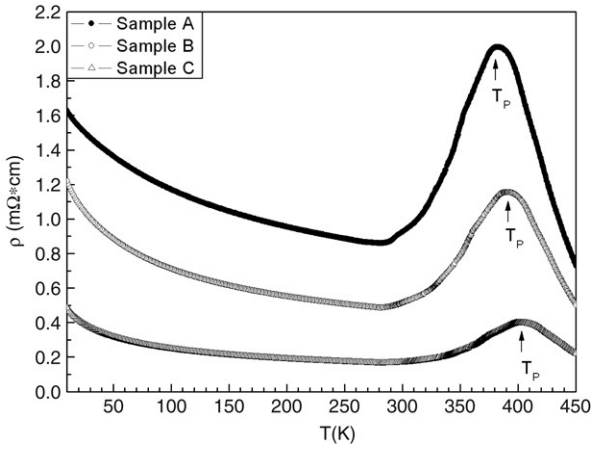

Fig. 6. The temperature dependence of the resistivity for polycrystalline Sr_2FeMoO_6 at zero field in the temperature range from 10 to 450 K.

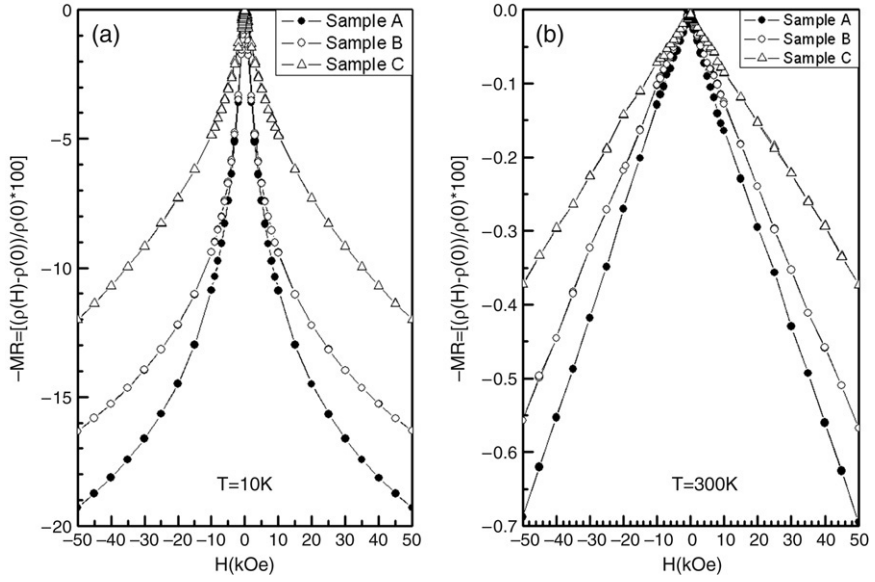

Fig. 7. The magnetic field dependence of the magnetoresistivity ratio from −5 to 5 T at 10 and 300 K.

antiphase boundaries and grain boundaries, e.g., the grain size, the connection between grains, and the crystallinity of the intragranular material, etc. [2,19–21]. The ideal sample with optimal low field magnetoresistence should have small grains with high saturation magnetization and high spin polarization [17]. For our samples, the grain size becomes larger and the crystallization becomes more perfect and the value of MR decreases with increase of the sintering temperature, as shown in Figs. 3 and 7. So the GB effects are more remarkable for the sample with the small grain size, caused by the lower sintering temperature. Further work on improving the Fe/Mo order as well as the low field MR and the transport properties is being carried out and will be reported elsewhere.

4. Conclusion

In conclusion, Sr_2FeMoO_6 samples with different grain sizes were prepared by the sol–gel method. The XRD patterns and SEM for the Sr_2FeMoO_6 samples show that the samples are in the nanometer range. The transport measurements show that the Sr_2FeMoO_6 samples behave like semiconductors at low temperatures, dominated by the carrier scattering at the grain boundaries. The temperature dependence of the magnetization and the resistance results clearly demonstrate the coexistence of ferromagnetic metallic and antiferromagnetic (or paramagnetic) insulating domains, which is believed to induce a metal–insulator transition at the Curie temperature. Further work on improving the Fe/Mo order as well as the low field magnetoresistance is being carried out and will be reported elsewhere.

Acknowledgements

This work was supported by the National Natural Science Foundation of China under contracts No. 10474100, No. 10374033 and No. 50672099, and the Director's Fund of Hefei Institutes of Physical Science, Chinese Academy of Sciences.

References

[1] G. Prinz, Science 282 (1998) 1660–1663.
[2] K. Kobayashi, T. Kimura, H. Sawada, K. Terakura, Y. Tokura, Nature 395 (1998) 677–680.
[3] L. Balcells, J. Navarro, M. Bibes, A. Roig, B. Martınez, J. Fontcuberta, Appl. Phys. Lett. 78 (2001) 781–783.
[4] Y. Tomioka, T. Okuda, Y. Okimoto, R. Kumai, K.I. Kobayashi, Phys. Rev. B 61 (2000) 422–427.
[5] D. Rubi, C. Frontera, A. Roig, J. Nogues, J.S. Munoz, J. Fontcuberta, Mater. Sci. Eng. B 126 (2006) 139–142.
[6] C.L. Yuan, S.G. Wang, W.H. Song, T. Yu, J.M. Dai, Y.P. Sun, Appl. Phys. Lett. 75 (1999) 3853–3855.
[7] Y.H. Huang, M. Karppinen, H. Yamauchi, J.B. Goodenough, Phys. Rev. B 73 (2006) 104408.
[8] M. García-Hernández, J.L. Martínez, M.J. Martínez-Lope, M.T. Casais, J.A. Alonso, Phys. Rev. Lett. 86 (2001) 2443–2446.
[9] M. Takashi, I. Makoto, K. Yoshinori, K.I. Kobayashi, Appl. Phys. Lett. 74 (1999) 2215–2217.
[10] X.B. Zhu, J.M. Dai, X.H. Li, B.C. Zhao, S.M. Liu, W.H. Song, Y.P. Sun, Mater. Lett. 59 (2005) 2366–2369.
[11] Y. Toshiaki, S. Hironori, K. Koichi, H. Shin-ichi, Solid State Commun. 133 (2005) 71–75.
[12] R.P. Borges, S. Lhostis, M.A. Bari, J.J. Versluijs, J.G. Lunney, J.M.D. Coey, M. Besse, J.-P. Contour, Thin Solid Films 429 (2003) 5–12.
[13] Y.H. Huang, H. Yamauchi, M. Karppinen, Phys. Rev. B 74 (2006) 174418.
[14] W.H. Song, J.M. Dai, S.L. Ye, K.Y. Wang, J.J. Du, Y.P. Sun, J. Appl. Phys. 89 (2001) 7678–7680.
[15] Falak Sher, A. Venimadhav, Mark G. Blamire, K. Kamenev, J. Paul Attfield, Chem. Mater. 17 (2005) 176–180.
[16] M.T. Causa, M. Tovar, A. Caneiro, F. Prado, G. Ibanez, C.A. Ramos, A. Butera, B. Alascio, X. Obradors, S. Pinol, F. Rivadulla, C. Vazquez-Vazquez, A. Lopez-Qintela, J. Rivas, Y. Tokuers, S.B. Oseroff, Phys. Rev. B 58 (1998) 3233–3239.
[17] Y.H. Huang, J. Linden, H. Yamauchi, M. Karppinen, Chem. Mater. 16 (2004) 4337–4342.
[18] C.L. Yuan, Z.Y. Zeng, Y. Zhu, P.P. Ong, Z.X. Shen, C.K. Ong, Cond-Mat. (2003) 0307527.
[19] T.T. Fang, Phys. Rev. B 71 (2005) 064401.
[20] W. Zhong, W. Liu, C.T. Au, Y.W. Du, Nanotechnology 17 (2006) 250–256.
[21] A. Sharma, A. Berenov, J. Rager, W. Branford, Y. Bugoslavsky, L.F. Cohen, J.L. MacManus-Driscoll, Appl. Phys. Lett. 83 (2003) 2384–2386.